









Cite this: *Chem. Commun.*, 2020, 56, 3567

Received 19th December 2019,
Accepted 20th February 2020

DOI: 10.1039/c9cc09849f

rsc.li/chemcomm

Synthesis and characterization of high affinity fluorogenic α -synuclein probes†

Zsolia Lengyel-Zhand, ^a John J. Ferrie, ^b Bienneke Janssen, ^a Chia-Ju Hsieh,^a Thomas Graham,^a Kui-ying Xu,^a Conor M. Haney, ^b Virginia M.-Y. Lee,^c John Q. Trojanowski,^c E. James Petersson ^{*b} and Robert H. Mach ^{*a}

Fluorescent small molecules are powerful tools for imaging α -synuclein pathology *in vitro* and *in vivo*. In this work, we explore benzofuranone as a potential scaffold for the design of fluorescent α -synuclein probes. These compounds have high affinity for α -synuclein, show fluorescent turn-on upon binding to fibrils, and display different binding to Lewy bodies, Lewy neurites and glial cytoplasmic inclusion pathologies in post-mortem brain tissue. These studies not only reveal the potential of benzofuranone compounds as α -synuclein specific fluorescent probes, but also have implications for the ways in which α -synucleinopathies are conformationally different and display distinct small molecule binding sites.

Insoluble protein aggregates are pathological hallmarks of many neurodegenerative disorders and have been used for identification at the time of autopsy.¹ Parkinson's disease (PD) and multiple system atrophy (MSA) are characterized by the abnormal deposition of α -synuclein (α -Syn) in multiple brain regions. In PD patients, α -Syn forms amyloid fibrils and accumulates in spherical shaped cytoplasmic inclusions, called Lewy bodies (LBs), and rod-shaped neuritic inclusions, called Lewy neurites (LNs).² By contrast, α -Syn is found within glial cytoplasmic inclusions (GCIs) in multiple system atrophy (MSA),³ and it has been reported that MSA patients possess pathological α -Syn with biochemical and biological properties distinct from those found in Lewy bodies and neurites.⁴

Currently, the detection of α -Syn and other amyloid deposits *in vitro* is commonly based on measuring enhanced fluorescence emission of probes upon binding to amyloid fibrils.⁵ Although

antibodies are the currently favored choice for detection of various amyloids,⁶ they are not suitable for studying the location and availability of binding sites in α -Syn fibrils, information that is crucial for the development of imaging probes and therapeutic agents targeting α -Syn inclusions. Besides antibodies, fluorescent small molecules are often used in imaging due to their favorable properties: small size, high sensitivity and physicochemical properties that can be readily fine-tuned.⁷ For the detection of amyloid fibrils, the most widely utilized fluorescent probes are Thioflavin S, the benzothiazole dye Thioflavin T (ThT) and the sulfonated azo dye Congo Red.⁸ Despite their favorable absorbance and fluorescent properties, these probes have significant drawbacks. They have low affinity for α -synuclein fibrils, often give false positive results and they cannot distinguish between α -Syn inclusions.⁹ These deficiencies have led to increased efforts to develop better probes for imaging α -Syn fibrils, since a small molecule that labels LB pathology with high affinity and does not label GCIs would greatly advance research for PD.¹⁰ As of today, a number of fluorescent molecules have been reported for binding to α -Syn fibrils.¹¹ Despite the progress that has been achieved in recent years, many of the reported fluorescent probes fail to distinguish between different forms of α -Syn (LB vs. GCIs) and have low affinity.^{5b}

Recently, we reported a series of (benzylidene)indolin-2-one derivatives that could serve as lead compounds for PET tracer development.¹² Most of the described compounds showed modest affinity for α -Syn fibrils and only a few displayed dissociation constants lower than 20 nM. Encouraged by the results, we set out to explore binding and fluorescent properties of the benzofuranone analogues of these compounds. Benzofuranone derivatives are promising scaffolds for the design of fluorescent probes, due to their favorable absorption and fluorescence properties.¹³ Herein we describe the synthesis and characterization of various benzofuranone analogues and we demonstrate for the first time that a small molecule can distinguish between LB, LN and GCI pathology in human post-mortem brain tissue.

The synthesis of the target compounds began with the preparation of **Tg-47** by reacting 5-hydroxybenzofuran-3-one

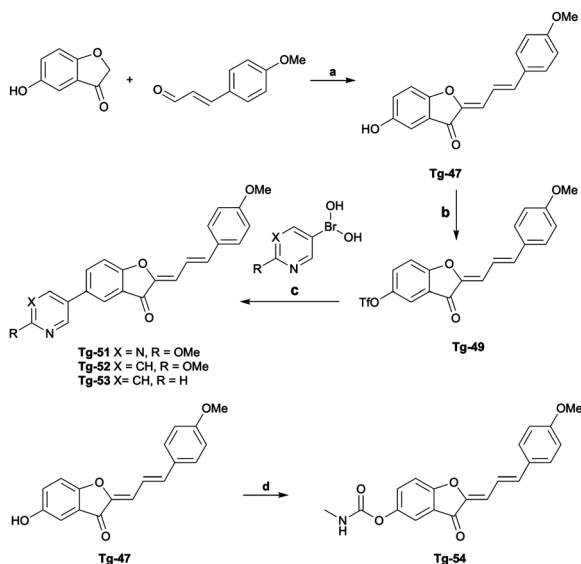
^a Department of Radiology, Perelman School of Medicine, University of Pennsylvania, Philadelphia, PA 19104, USA. E-mail: rmach@pennmedicine.upenn.edu

^b Department of Chemistry, University of Pennsylvania, Philadelphia, Pennsylvania 19104, USA. E-mail: ejamesp@sas.upenn.edu

^c Department of Pathology and Laboratory Medicine, Perelman School of Medicine, University of Pennsylvania, Philadelphia, PA 19104, USA

† Electronic supplementary information (ESI) available. See DOI: 10.1039/c9cc09849f
‡ These authors contributed equally.

* Current address: Department of Chemistry and Biochemistry, University of North Carolina Wilmington, Wilmington, NC 28403, USA.



Scheme 1 Synthesis of benzofuranone analogues. *Reagents and conditions: (a) HCl, EtOH, 70 °C, 3 h (52%) (b) pyridine, Tf₂O, CH₂Cl₂, rt, 30 min (94%); (c) XPhos Pd G2, K₃PO₄, dioxane/H₂O, 50 °C, 20 min (**Tg-51** 76%; **Tg-52** 80%; **Tg-53** 49%); (d) TEA, DMAP, *N*-methylcarbamoyl chloride, rt, 2 h (49%).

with 4-methoxycinnamaldehyde, which was then converted to trifluoromethanesulfonate ester **Tg-49** (Scheme 1). Next, we incorporated various substituents on the aromatic ring to determine if these groups would improve the affinity and fluorescence properties of these compounds. A Suzuki cross coupling between triflate **Tg-49** and the appropriate (hetero)aryl boronic acid was performed to obtain benzofuranone analogs **Tg-51–53**. The methylcarbamate analogue **Tg-54** was synthesized by reacting **Tg-47** with *N*-methylcarbamoyl chloride. The final compounds were obtained as yellow/orange solids with purity > 95%.

Previously we identified putative binding sites, sites 2 and 9 (Fig. S1b in ESI†), for small molecules on α -Syn fibrils.¹⁴ In order to access the binding site of the benzofuranone derivatives and determine their binding energy, we performed computational docking studies. The NMR structure of α -Syn fibrils (PDB: 2N0A)¹⁵ was imported from the Protein Data Bank and molecular blind docking studies were conducted *via* the AutoDock PyMOL plugin.¹⁶ All four compounds favored both sites 2 and 9 with **Tg-54** being the least and **Tg-52** being the most potent binder (Table S1 in ESI†). The interactions of the compounds with binding sites 2 and 9 are shown in Fig. S1–S3 in the ESI†.

Next, we set out to determine the affinity of **Tg-51–54** for α -Syn fibrils. Our recent work highlights two compounds, [³H]-Tg-190b and [³H]-BF2846 (Fig. S4a in ESI†) that selectively bind to site 2 and site 9, respectively, and can be utilized in radioligand competition binding assays to measure the affinity of α -Syn ligands. The binding assay measured the displacement of these radioligands by increasing concentrations of competitor compounds, using fixed concentrations of fibrils and radioligand. **Tg-51–53** displayed remarkably high affinity for site 2 of α -Syn fibrils and a slightly lower affinity for site 9, with **Tg-52** being the most potent and having an inhibitory concentration (IC₅₀) of

Table 1 Comparison of IC₅₀ and K_i values for binding to site 2 or site 9 in α -Syn fibrils

Compound	Site 2	Site 9
	IC ₅₀ ^a (nM)	K _i ^a (nM)
Tg-51	25.8 (13.4–51.1)	18.3 (8.10–42.7)
Tg-52	1.18 (0.394–4.03)	2.32 (1.56–3.42)
Tg-53	38.6 (16.1–92.0)	33.8 (18.0–64.9)
Tg-54	222 (102–492)	35.1 (25.0–49.7)

^a Values were determined by competition binding assay with [³H]-Tg-190b or [³H]-BF2846. 95% confidence intervals for IC₅₀ and K_i values are shown in parentheses (*n* = 3).

1.18 nM for site 2 and an inhibitor constant (K_i) of 2.32 nM for site 9 (Table 1 and Fig. S4b in ESI†). The affinity of **Tg-52** is several orders of magnitude higher than the commonly used dye, thioflavin T (Table S2 in ESI†). Replacing the pyridine ring with an *N*-methyl carbamate group (**Tg-54**) resulted in decreased affinity for site 2 and slightly lower affinity to site 9 compared to **Tg-51–52**. This is likely due to the lack of π - π stacking between the pyridine group and the tyrosine 39 residue of the fibrils, which could further stabilize the interaction. The results are consistent with the docking studies and confirm that these benzofuranone derivatives are suitable α -Syn ligands with high affinity.

We studied the fluorescence properties of these benzofuranone analogs to determine their efficacy as probes for biological applications. All compounds showed an absorption maximum in the visible range in 50:50 tris buffer/DMSO, and the absorbance maxima were all within ± 2 nm (Fig. 1a and Fig. S5 in ESI†). Curiously, the absorbance maximum of **Tg-51** was blue-shifted by ~ 70 nm for absorbances measured at higher concentrations. Overall, the various substitutions on the aromatic rings did not show a marked effect on the absorption maxima (Table S3 in ESI†). The spectra of all compounds display a bathochromic shift after binding to fibrils, which has been observed for other fibril binding compounds. For ThT, spectral shifts in the molecule's absorbance profile associated with fibril binding have been attributed to differences in the local dielectric forces experienced by the molecule when free in solution *versus* bound to the fibril surface.¹⁷ Alternatively, binding of Congo Red to fibrils results in an extension of the π -system, producing the observed red-shift.¹⁸ Since, the absorbance maxima of these compounds revealed similar, ~ 10 nm shifts, due to both fibril binding and variations in solvent polarity for unbound compounds, the bathochromic shift upon fibril binding is likely the result of changes in local polarity (Fig. S6 in ESI†). Moreover, the more pronounced shift observed from **Tg-51** binding is also likely attributable to changes in local polarity, as all compounds display significant hypsochromic shifts in the presence of high polarity solvents (Fig. S6–S8 in ESI†).

Next, we measured the molar extinction coefficients (ϵ) of the various analogs free in solution and bound to fibrils (Fig. S7 in ESI†). The values of ϵ at each compounds' absorption maximum are summarized in Table S3 in ESI†. The extinction coefficients of **Tg-51** and **Tg-52** were significantly smaller than those of **Tg-53** and **Tg-54**, however we observed that the absorbance of all four compounds increased upon binding to

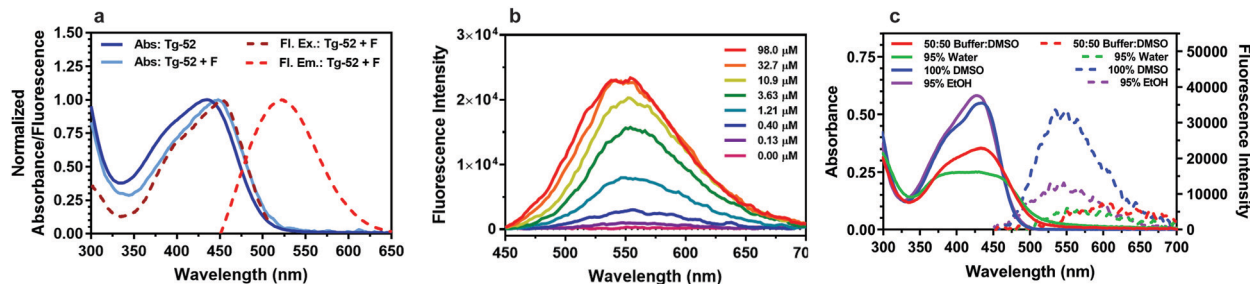


Fig. 1 (a) Absorbance and emission spectra of **Tg-52** free in solution and bound to fibrils. Absorbance spectra free in solution (blue solid line) and bound to α -Syn fibrils (light-blue solid line) and fluorescence excitation spectrum (dark red dashed line) and emission spectrum (red dashed line) were acquired with 1 μ M of **Tg-52** and 98 μ M α -Syn fibrils. (b) Determination of fluorescence turn-on of **Tg-52** upon fibril binding. Fluorescence emission spectra were acquired for 1 μ M **Tg-52** in the presence of serial dilutions of α -Syn fibrils. (c) Determination of absorbance and fluorescence sensitivity to environmental polarity. Absorbance (solid lines) and fluorescence spectra (dashed lines) of 20 μ M and 5 μ M **Tg-52**, respectively, in various solvent conditions.

α -Syn. Moreover, the extinction coefficients were highly sensitive to changes in polarity, where low polarity solvents afforded increases in absorbance (Fig. S6 in ESI[†]). The fluorescence emission spectra of the compounds showed a maximum between 522 and 534 nm. All four ligands are practically non-fluorescent in water. Upon mixing with α -Syn fibrils, a pronounced increase in fluorescence intensity was observed (Fig. 1b and Fig. S8 in ESI[†]). The high turn-on associated with binding of these compounds enabled us to facilitate measure their relative binding affinities by fluorometric titration. The emission of compounds was measured in the presence of varying concentrations of α -Syn fibrils and the total intensity from either excitation or emission spectra was plotted as a function of fibril concentration (Fig. S8 in ESI[†]), with **Tg-52** displaying the highest relative affinity (Table S4 in ESI[†]). To further characterize the spectroscopic properties of the benzofuranone analogs, fluorescence quantum yields were determined *via* comparison to ThT (Fig. S9 in ESI[†]). **Tg-51** showed the highest quantum yield when bound to fibrils, followed by **Tg-53** (Table S3 in ESI[†]). Thus, binding in the less polar fibril pocket will lead to an increase in brightness due to changes in extinction coefficient and quantum yield (Fig. 1c and Fig. S6 in ESI[†]), but this does not fully account for the increase in fluorescence observed during fibril binding. Therefore, we suspect that restriction of the numerous degrees of rotational and vibrational freedom associated with fibril binding reduces non-emissive relaxation from the excited state, resulting in the noted fluorescence turn-on associated with binding. Lastly, we measured the fluorescence lifetime of the designed compounds when bound to α -Syn fibrils. (Fig. S10 in ESI[†]) The measured lifetimes ranged between 1.00 and 1.16 ns, with **Tg-52** exhibiting the longest lifetime of 1.16 ns (Table S3 in ESI[†]).

The favorable fluorescence properties of these compounds and their high affinity for α -Syn fibrils encouraged us to investigate *in vitro* fluorescent staining of post-mortem brain samples from anecdotal cases of PD, AD and MSA patients. We chose **Tg-52** to test as a biological probe due to its high affinity for α -Syn fibrils. Sections from frontal cortex tissue of PD and AD cases and cerebellum tissue of MSA cases were incubated with 10 μ M **Tg-52** and imaged using a fluorescence microscope (Fig. 2). Immunostaining with Syn303, a pan- α -Syn antibody known to detect a variety of types of aggregates,^{6b} was performed on

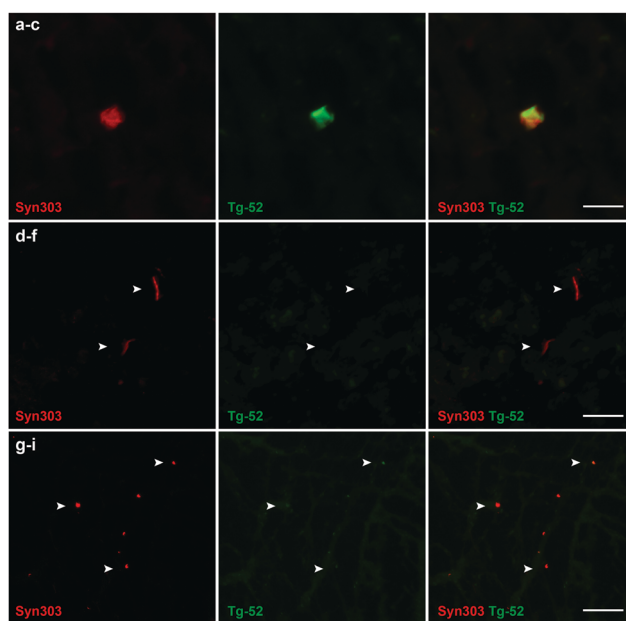


Fig. 2 Fluorescence microscopy studies of compound **Tg-52** in post-mortem samples of PD and MSA brain. Images show LBs (a–c), LNs (d–f) and GCIs (g–i) immunostained with Syn303 antibody and **Tg-52**. The fluorescent compound shows high labeling of LBs, weak labeling of GCIs and does not label LNs. [scale bars, 50 μ m (c), 65 μ m (f) and 100 μ m (i)].

the same section to determine the protein species labeled by the fluorescent probe.

Tg-52 displays high labeling of LBs in PD brain sections and α β plaques in AD sections (Fig. 2a–c and Fig. S11, S12 in ESI[†]), however it did not label LNs and displayed weak labeling of GCIs in MSA brain sections (Fig. 2d–i and Fig. S11 in ESI[†]), suggesting that these α -Syn inclusions have distinct binding sites available for small molecules. Understanding the location of these binding sites is crucial in designing therapeutic agents and small molecule imaging probes for PD and our data imply that site 2 and site 9 of α -Syn are not readily available in LNs and GCIs. However, further studies are merited to better understand the different available binding sites in Lewy bodies and neurites.

In conclusion, we have developed small molecule fluorescent probes for imaging α -Syn pathology, using benzofuranone as a

core structure. The synthesized compounds show high affinity for α -Syn fibrils *in vitro* and have favorable fluorescent properties. The compounds display a fluorescent turn-on: they are non-fluorescent in water and have increased fluorescence intensity upon binding to fibrils, making them highly useful α -Syn probes for cellular and tissue imaging. The difference in labeling α -Syn pathology in post-mortem brain tissue implies that α -synucleinopathies are conformationally different and possess distinct small molecule binding sites. Future studies will focus on better understanding the available binding sites in α -Syn pathology and also increasing the selectivity of these compounds toward α -Syn. Given the relatively low abundance of LB in PD tissue, it is likely that a successful probe or therapeutic agent targeting α -Syn will need to be capable of engaging a small molecule binding site present within both LBs and LNs. We envision that emerging cryo-electron microscopy studies of α -Syn from PD patients will guide the design and development of new imaging probes and therapeutic agents by providing a clearer picture of the available binding sites.

This research was supported by the National Institutes of Health (NIH NS103873 to EJP and AG10124 and AG062418 to JQT and VMYL) and the Michael J. Fox Foundation (to RHM). Instruments supported by the NIH and National Science Foundation include NMR (NSF CHE-1827457) and mass spectrometers (NIH RR-023444 and NSF MRI-0820996). JJF thanks the NSF (DGE-1321851) and the Parkinson's Disease Foundation (PF-RVSA-SFW-1754) for fellowship support. CMH was supported by an Age-Related Neurodegenerative Disease Training Grant fellowship (NIH T32AG000255).

Conflicts of interest

There are no conflicts to declare.

Notes and references

- 1 D. M. Skovronsky, V. M.-Y. Lee and J. Q. Trojanowski, *Annu. Rev. Pathol.: Mech. Dis.*, 2006, **1**, 151–170.
- 2 (a) M. G. Spillantini, M. L. Schmidt, V. M.-Y. Lee, J. Q. Trojanowski, R. Jakes and M. Goedert, *Nature*, 1997, **388**, 839; (b) C. F. Lippa, H. Fujiwara, D. M. Mann, B. Giasson, M. Baba, M. L. Schmidt, L. E. Nee, B. O'Connell, D. A. Pollen and P. S. George-Hyslop, *Am. J. Pathol.*, 1998, **153**, 1365–1370.
- 3 P. h. Tu, J. E. Galvin, M. Baba, B. Giasson, T. Tomita, S. Leight, S. Nakajo, T. Iwatsubo, J. Q. Trojanowski and V. M. Y. Lee, *Ann. Neurol.*, 1998, **44**, 415–422.
- 4 (a) J. L. Guo, D. J. Covell, J. P. Daniels, M. Iba, A. Stieber, B. Zhang, D. M. Riddle, L. K. Kwong, Y. Xu and J. Q. Trojanowski, *Cell*, 2013, **154**, 103–117; (b) W. Peelaerts, L. Bousset, A. Van der Perren, A. Moskalyuk, R. Pulizzi, M. Giugliano, C. Van den Haute, R. Melki and V. Baekelandt, *Nature*, 2015, **522**, 340; (c) C. Peng, R. J. Gathagan, D. J. Covell, C. Medellin, A. Stieber, J. L. Robinson, B. Zhang, R. M. Pitkin, M. F. Olufemi and K. C. Luk, *Nature*, 2018, **557**, 558; (d) S. B. Prusiner, A. L. Woerman, D. A. Mordes, J. C. Watts, R. Rampersaud, D. B. Berry, S. Patel, A. Oehler, J. K. Lowe and S. N. Kravitz, *Proc. Natl. Acad. Sci. U. S. A.*, 2015, **112**, E5308–E5317.
- 5 (a) A. Sulatskaya, N. Rodina, M. Sulatsky, O. Povarova, I. Antifeeva, I. Kuznetsova and K. Turoverov, *Int. J. Mol. Sci.*, 2018, **19**, 2486; (b) H. M. Lai, W.-L. Ng, S. M. Gentleman and W. Wu, *Cell Chem. Biol.*, 2017, **24**, 659–672; (c) S. Lim, M. M. Haque, D. Su, D. Kim, J.-S. Lee, Y.-T. Chang and Y. K. Kim, *Chem. Commun.*, 2017, **53**, 1607–1610.
- 6 (a) E. R. Greiner, J. W. Kelly and F. L. Palhano, *PLoS One*, 2014, **9**, e105433; (b) D. Covell, J. Robinson, R. Akhtar, M. Grossman, D. Weintraub, H. Bucklin, R. Pitkin, D. Riddle, A. Yousef and J. Trojanowski, *Neuropathol. Appl. Neurobiol.*, 2017, **43**, 604–620.
- 7 (a) J. B. Grimm, A. K. Muthusamy, Y. Liang, T. A. Brown, W. C. Lemon, R. Patel, R. Lu, J. J. Macklin, P. J. Keller and N. Ji, *Nat. Methods*, 2017, **14**, 987; (b) A. A. Reinke, H. Y. Seh and J. E. Gestwicki, *Bioorg. Med. Chem.*, 2009, **19**, 4952–4957.
- 8 M. R. Nilsson, *Methods*, 2004, **34**, 151–160.
- 9 (a) W. E. Klunk, Y. Wang, G.-F. Huang, M. L. Debnath, D. P. Holt and C. A. Mathis, *Life Sci.*, 2001, **69**, 1471–1484; (b) H. LeVine, *Amyloid*, 1995, **2**, 1–6; (c) C. Xue, T. Y. Lin, D. Chang and Z. Guo, *R. Soc. Open Sci.*, 2017, **4**, 160696; (d) R. Khurana, V. N. Uversky, L. Nielsen and A. L. Fink, *J. Biol. Chem.*, 2001, **276**, 22715–22721.
- 10 P. T. Kotzbauer, Z. Tu and R. H. Mach, *Clin. Transl. Imaging*, 2017, **5**, 3–14.
- 11 (a) J. V. Jun, C. M. Haney, R. J. Karpowicz Jr, S. Giannakoulis, V. M.-Y. Lee, E. J. Petersson and D. M. Chenoweth, *J. Am. Chem. Soc.*, 2019, **141**, 1893–1897; (b) K. L. Neal, N. B. Shakerdige, S. S. Hou, W. E. Klunk, C. A. Mathis, E. E. Nesterov, T. M. Swager, P. J. McLean and B. J. Bacskai, *Mol. Imaging Biol.*, 2013, **15**, 585–595; (c) V. Kovalska, M. Y. Losytskyy, O. Tolmachev, Y. L. Slominskii, G. M. Segers-Nolten, V. Subramaniam and S. Yarmoluk, *J. Fluoresc.*, 2012, **22**, 1441–1448; (d) C. W. T. Leung, F. Guo, Y. Hong, E. Zhao, R. T. K. Kwok, N. L. C. Leung, S. Chen, N. N. Vaikath, O. M. El-Agnaf and Y. Tang, *Chem. Commun.*, 2015, **51**, 1866–1869; (e) M. S. Celej, W. Caarls, A. P. Demchenko and T. M. Jovin, *Biochemistry*, 2009, **48**, 7465–7472; (f) M. S. Celej, E. A. Jares-Erijman and T. M. Jovin, *Biophys. J.*, 2008, **94**, 4867–4879; (g) K. D. Volkova, V. Kovalska, A. Balanda, M. Y. Losytskyy, A. Golub, R. Vermeij, V. Subramaniam, O. Tolmachev and S. Yarmoluk, *Bioorg. Med. Chem.*, 2008, **16**, 1452–1459.
- 12 W. Chu, D. Zhou, V. Gaba, J. Liu, S. Li, X. Peng, J. Xu, D. Dhavale, D. P. Bagchi and A. d'Avignon, *J. Med. Chem.*, 2015, **58**, 6002–6017.
- 13 C. Espinosa-Bustos, D. Cortés-Arriagada, M. A. Soto-Arriaza, J. Robinson-Duggon, N. Pizarro, A. R. Cabrera, D. Fuentealba and C. O. Salas, *Photochem. Photobiol. Sci.*, 2017, **16**, 1268–1276.
- 14 C.-J. Hsieh, J. J. Ferrie, K. Xu, I. Lee, T. J. Graham, Z. Tu, J. Yu, D. Dhavale, P. Kotzbauer and E. J. Petersson, *ACS Chem. Neurosci.*, 2018, **9**, 2521–2527.
- 15 M. D. Tuttle, G. Comellas, A. J. Nieuwkoop, D. J. Covell, D. A. Berthold, K. D. Kloepper, J. M. Courtney, J. K. Kim, A. M. Barclay and A. Kendall, *Nat. Struct. Mol. Biol.*, 2016, **23**, 409.
- 16 G. M. Morris, R. Huey, W. Lindstrom, M. F. Sanner, R. K. Belew, D. S. Goodsell and A. J. Olson, *J. Comput. Chem.*, 2009, **30**, 2785–2791.
- 17 A. A. Maskevich, V. I. Stsiapura, V. A. Kuzmitsky, I. M. Kuznetsova, O. I. Povarova, V. N. Uversky and K. K. Turoverov, *J. Proteome Res.*, 2007, **6**, 1392–1401.
- 18 T. Miura, C. Yamamiya, M. Sasaki, K. Suzuki and H. Takeuchi, *J. Raman Spectrosc.*, 2002, **33**, 530–535.